Nonlinear hysteretic behavior of a confined sliding layer

N. Manini[1,2], **G.E. Santoro**[2,3], **E. Tosatti**[2,3], **and A. Vanossi**[4]

[1]Dipart. di Fisica and CNR-INFM, Università di Milano, Via Celoria 16, 20133 Milano, Italy
[2]International School for Advanced Studies (SISSA) and CNR-INFM Democritos National Simulation Center, Via Beirut 2-4, I-34014 Trieste, Italy
[3]International Centre for Theoretical Physics (ICTP), P.O.Box 586, I-34014 Trieste, Italy
[4]CNR-INFM National Research Center S3 and Department of Physics, University of Modena and Reggio Emilia, Via Campi 213/A, 41100 Modena, Italy

Abstract. A nonlinear model representing the tribological problem of a thin solid lubricant layer between two sliding periodic surfaces is used to analyze the phenomenon of hysteresis at pinning/depinning around a moving state rather than around a statically pinned state. The cycling of an external driving force F_{ext} is used as a simple means to destroy and then to recover the dynamically pinned state previously discovered for the lubricant center-of-mass velocity. De-pinning to a quasi-freely sliding state occurs either directly, with a single jump, or through a sequence of discontinuous transitions. The intermediate sliding steps are reminiscent of phase-locked states and stick-slip motion in static friction, and can be interpreted in terms of the appearance of travelling density defects in an otherwise regular arrangement of kinks. Re-pinning occurs more smoothly, through the successive disappearance of different travelling defects. The resulting bistability and multistability regions may also be explored by varying mechanical parameters other than F_{ext}, e.g. the sliding velocity or the corrugation amplitude of the sliders.

1. Introduction

Nonlinear systems driven far from equilibrium exhibit a very rich variety of complex spatial and temporal behaviors [1]. In particular, in the emerging field of nanoscale science and technology, understanding the nonequilibrium dynamics of systems with many degrees of freedom which are pinned in some periodic potential, as is commonly the case in solid-state physics, is often becoming an issue. Friction belongs to this category too, because the microscopic corrugation of the mating surfaces may interlock [2, 3]. Simple phenomenological models are important, as they often give not only qualitative understanding of experimental findings, but also fair quantitative agreement with nanoscale tribology data, and with realistic simulations of sliding phenomena [4]. In this line of simplified approaches, studies are typically restricted to describing microscopic dynamics in one (1D) or two (2D) spatial dimensions. The substrates defining the moving interface are modelled in a simplified way as purely rigid surfaces or as one- or two-dimensional arrays of particles interacting through simple (e.g., harmonic) potentials. Despite such a crude level of description, this class of approaches frequently reveals the ability of modelling the main features of the complex microscopic dynamics, ranging from regular to chaotic motion [5, 6, 7].

One of the pervasive concepts of modern tribology – with a wide area of relevant practical applications as well as fundamental theoretical issues – is the idea of free sliding connected

with *incommensurability*. When two crystalline workpieces with incommensurate or misaligned lattices are brought into contact, the minimal force required to achieve sliding, i.e. the static friction, should vanish, at least provided the two crystals are stiff enough. In such a geometrical configuration, the lattice mismatch can prevent interlocking of the two periodic corrugations and the resulting collective stick-slip motion of the interface atoms, with a consequent dramatically reduced frictional force. Experimental observation of this sort of *superlubric* and anisotropic regime of motion has been reported recently [8, 9]. The paradigm of frictionless sliding is realized naturally by the 1D Frenkel-Kontorova (FK) model (see Ref. [5] and references therein). However the physical contact between two solids is generally mediated by so-called "third bodies", and the role of incommensurability has been recently extended [10] in the framework of a driven 1D model inspired by the tribological problem of two sliding interfaces with a thin solid lubricant layer in between. The frictional interface is thus characterized by *three* inherent length scales along the sliding direction: the periods of the bottom and top substrates, and the period of the embedded solid lubricant structure. In particular, in the presence of a uniform external driving velocity, the interplay of these incommensurate length scales can give rise to intriguing dynamical phase locking phenomena and surprising velocity quantization effects [11, 12].

Previous numerical and theoretical studies of this confined tribological model [11, 12, 13] discovered a quantization of the lubricant center-of-mass (CM) relative velocity and found it to be related to the pinning of topological density excitations (kinks) to the substrate of closest periodicity. More recent work [14] highlighted a strict analogy of these dynamical pinning phenomena to the ordinary commensurate pinning of *static* friction [15, 16]. The proposed mapping between this dynamical pinning and that of static friction was explored numerically by analyzing the effect of an additional external driving force F_{ext}, equal for all lubricant particles. Dynamical pinning is signified by the lubricant CM relative velocity remaining robustly locked to the quantized plateau value (a value strictly and analytically determined by spatial periodicity ratios alone) up to a critical force threshold, above which quantization is destroyed.

It was also found that as long as inertial effects are non negligible compared to dissipative forces (*underdamped* regime of motion), the adiabatic variation (increase and decrease) of the external driving force gives rise to a large hysteresis loop in the v_{cm} – F_{ext} characteristics, not unlike depinning in static friction [5, 15]. The present paper focuses precisely on the hysteretic behavior around a dynamical quantized steady state that this system exhibits, and discuss similarities and differences between such a dynamical locking and the more usual static pinning. By exploiting configurations where the dynamics of individual kinks is easy to monitor visually, the mechanism of hysteresis will be clarified. Given the practical difficulty of an experimental setup where an equal driving force is applied to each lubricant particle on the fly, the F_{ext} term is may be seen more as a useful mathematical device rather than a realistic suggestion for future measurements aimed at studying dynamical depinning. On the other hand, we will bring concrete examples of the hysteretical destruction and recovery of the CM velocity plateau by means of parameters other than F_{ext} being cycled. The cycling of the substrate sliding velocity or of the applied load sketch practical possibilities to address the dynamical hysteresis in experimental tribological investigations.

2. Confined lubricant model: numerical simulations

We will work with the one-dimensional generalization of the standard FK model introduced in Ref. [11, 12], consisting of two rigid sinusoidal substrates, of spatial periodicity a_+ and a_-, and a chain of harmonically interacting particles, of equilibrium length a_0, mimicking the sandwiched lubricant layer, as sketched in the inset of Fig. 1.[1] The two substrates move at a constant

---

[1] The harmonicity of interactions within the lubricant chain is merely a simplifying assumption, since test simulations with anharmonic inter-particle potentials (e.g. Morse and Lennard-Jones) also reveal the ubiquity of the observed phenomenology.
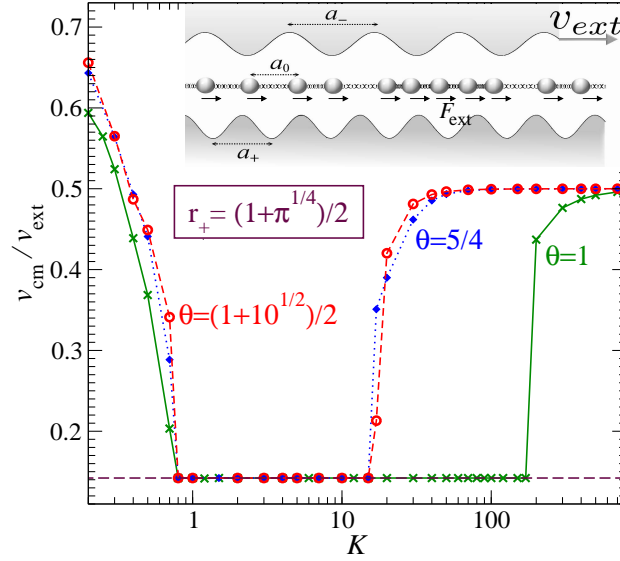
Figure 1. (Color online) Normalized velocity of the center of mass, $v_{\mathrm{cm}}/v_{\mathrm{ext}}$, as a function of the chain stiffness KF_+/a_+, for $v_{\mathrm{ext}} = 0.1\,(F_+a_+/m)^{1/2}$, $\gamma = 0.1\,(F_+m/a_+)^{1/2}$, and $r_+ = (1 + \pi^{1/4})/2$. Crosses: one-to-one kink coverage $\theta = 1$ ($r_- \simeq 7.036$); diamonds: commensurate kink coverage $\theta = 5/4$ ($r_- \simeq 8.795$); circles: incommensurate kink coverage $\theta = (1 + 10^{1/2})/3$ ($r_- \simeq 9.762$). Dashed line: the quantized-plateau velocity ratio of Eq. (2). Note the logarithmic scale in the abscissa. Inset: a sketch of the driven 3-lengthscale confined model.

relative velocity $v_{\mathrm{ext}} = v_- - v_+$. In particular, we select the reference frame where $v_+ = 0$ and $v_- = v_{\mathrm{ext}}$. The equation of motion of the i-th lubricant particle is:

$$
m\ddot{x}_i = -\frac{1}{2}\left[F_+ \sin\frac{2\pi}{a_+}x_i + F_- \sin\frac{2\pi}{a_-}(x_i - v_{\mathrm{ext}}t)\right]
$$
$$
+K(x_{i+1} + x_{i-1} - 2x_i) - 2\gamma(\dot{x}_i - v_{\mathrm{w}}) + F_{\mathrm{ext}} , \tag{1}
$$

where m is its mass. $F_\pm$ are the amplitudes of the forces due to the sinusoidal corrugation of the substrates. By default, we set $F_-/F_+ = 1$ as the least biased choice, but we will explore the effect of modifying F_- in Sect. 3 below. K is the chain spring constant defining the harmonic nearest-neighbor interparticle interaction. The penultimate damping term in Eq. (1) originates from two symmetric frictional contributions adding as follows: $-\gamma\,(\dot{x}_i - v_+) - \gamma\,(\dot{x}_i - v_-) = -2\gamma\,(\dot{x}_i - \frac{1}{2}v_{\mathrm{ext}})$, where γ is a viscous friction coefficient accounting phenomenologically for degrees of freedom inherent in the real physical system (such as substrate phonons, electronic excitations, etc.) which are not explicitly included in the model; this fixes the reference speed of the the dissipative term: $v_{\mathrm{w}} = \frac{1}{2}v_{\mathrm{ext}}$ [2]. In order to probe the strength of quantization, and eventually address hysteresis, an additional constant force F_{ext} is applied to all chain particles and varied up and down adiabatically. The infinite chain size is managed – in the general incommensurate case – by means of periodic boundary conditions (PBC) and finite-size scaling [13]. We set overall $a_+ = 1$, $m = 1$, and $F_+ = 1$ as basic dimensionless units, and express implicitly all mechanical quantities in terms of natural model units obtained as combinations of these three basic units [13].

---

[2] We choose this value of the velocity $v_{\mathrm{w}} = \frac{1}{2}v_{\mathrm{ext}}$ to which dissipation refers as the least biased option. Different choices, equivalent to choosing different γ_+ and γ_- dissipation coefficients to the two substrates, would at most change the quantitative details of the velocity-plateau boundaries, but not the qualitative nature of results.

As previously found [11, 12, 13, 14] the detailed behavior of the driven system in Eq. (1) depends crucially on the relative (in)commensurability of the substrates and the chain. The relevant length ratios are defined by $r_\pm = a_\pm/a_0$; we assume $r_- > \min(r_+, r_+^{-1})$, whereby the (+) substrate has the closest periodicity to the lubricant, the (−) slider the furthest. Under rather general dynamical conditions, the lubricant slides with a quantized mean velocity v_{plateau} relative to the (+) substrate. The plateau phenomenon was explained by the static pinning of the topological solitons (kinks) that the embedded chain forms with the (+) substrate, to the (−) slider [11, 13]. Specifically, the quantized-plateau lubricant velocity ratio

$$\frac{v_{\mathrm{cm}}}{v_{\mathrm{ext}}} = \frac{v_{\mathrm{plateau}}}{v_{\mathrm{ext}}} \equiv 1 - \frac{1}{r_+}, \tag{2}$$

is strictly a function of the lubricant coverage r_+ of the (+) substrate [11], i.e. of the absolute density $(r_+ - 1)/a_+$ of kinks. For antikinks, $r_+ < 1$, this density is negative, and so is $v_{\mathrm{plateau}}-$ namely the lubricant slides *backwards* [11]. Although the quantized-plateau velocity depends uniquely on r_+, the plateau dynamical stability and extension depend crucially on the kink coverage

$$\theta = a_- \frac{r_+ - 1}{a_+} = r_- \left(1 - \frac{1}{r_+}\right) \tag{3}$$

of the (−) substrate (for antikinks, $\theta < 0$). Concretely, as a function, e.g. of the spring stiffness K, the quantized plateau is very prominent in a range of K of the order unity but weakens and eventually terminates for stiffer chains (larger K values), Fig. 1. The plateau destabilization is complete for a general irrational θ, while, under suitable conditions detailed below, the plateau can survive up to indefinitely large K for commensurate kink coverage (rational θ). The quantized velocity plateau is finally particularly robust for perfect one-to-one matching of the soliton and the (-) slider periodicities, $\theta = 1$ [14]. To illustrate these three typical cases, we consider $r_+ = (1 + \pi^{1/4})/2 \simeq 1.166$ and the three values $r_- \equiv \theta (1 - r_+^{-1})^{-1} \simeq 7.036, 8.795,$ and 9.762, corresponding to the values $\theta = 1$, $\theta = 5/4 = 1.250$, and $\theta = (1 + 10^{1/2})/3 \simeq 1.387$ respectively. The choice of r_+ near unity, is especially advantageous compared to values like the golden mean $(1 + \sqrt{5})/2 \simeq 1.618$ often used, because it gives rise to well-separated individual kinks, which allow a more transparent analysis of the dynamics. Many qualitative features discussed for the specific ratios $r_\pm$ considered here are in fact also found for general values of $r_\pm$, and thus this specific choice of length ratios should not be considered especially restrictive, as long as a correct distinction of different commensuration property of θ, Eq. (3), is made.

The equations of motion (1) are integrated using a standard fourth-order Runge-Kutta algorithm. The system is initialized with the chain particles placed at rest at uniform separation a_0, and the top substrate is made slide at the imposed constant velocity $v_- = v_{\mathrm{ext}}$. For $F_{\mathrm{ext}} = 0$ and a wide range of model parameters, after an initial transient the system reaches a steady state, where all dynamical quantities other than particle positions fluctuate but show no systematic drift. For wide ranges of parameters, exemplified in Fig. 1 by the spring stiffness K, the lubricant reaches the expected plateau state of normalized time-averaged velocity $v_{\mathrm{plateau}}/v_{\mathrm{ext}} \simeq 0.142$, Eq. (2), the same for the three geometries introduced above.

Adiabatic upward and downward variation of the external force F_{ext} is realized by changing F_{ext} in small steps and letting the system evolve at each step for a time long-enough for all transient stresses to relax. This allows us to gauge the robustness of the plateau state as a function of the system parameters, e.g. of K. In order to determine the critical values of F_{ext}, where the plateau is abandoned and retrieved, and in particular to do that with great accuracy and a reasonably small number of separate simulations, we first increment F_{ext} in steps of $0.01\, F_+$, and then reduce the step width using a bisection scheme around the critical force.

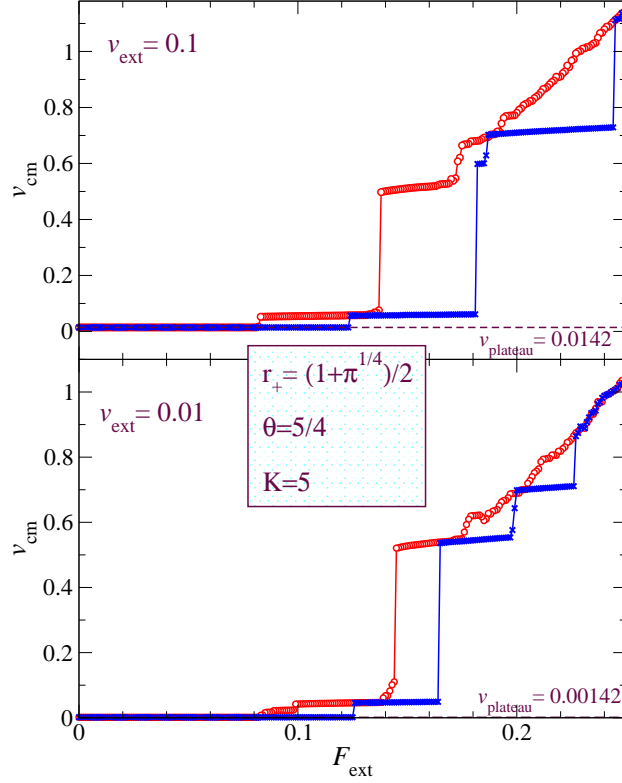**Figure 2.** (Color online) Hysteresis in the $v_{cm} - F_{ext}$ characteristics for a confined chain of intermediate spring stiffness ($K = 5F_+/a_+$), and length ratios $r_+ = (1 + \pi^{1/4})/2$, $\theta = 5/4$ ($r_- \simeq 8.795$). The behavior is shown for fast ($v_{ext} = 0.1$, upper panel) and slow ($v_{ext} = 0.01$, lower panel) drive. Adiabatic increase and decrease of F_{ext} (in steps of $10^{-3}F_+$) are denoted by crosses and circles, respectively. Characteristic hysteretic multi-step features appear. Here $\gamma = 0.1(F_+m/a_+)^{1/2}$, and a chain of $N = 387$ lubricant particles is simulated.

3. Results

For concreteness, we begin with the specific example $\theta = 5/4$, and pick an intermediate value of the chain stiffness $K = 5\,F_+/a_+$, common to all plateaus of Fig. 1. We start investigating the plateau destruction/recovery induced by varying the external force F_{ext} through a sequence of adiabatic increases and decreases [17]. The resulting CM velocity is displayed in Fig. 2 for two different external driving velocities v_{ext}. A clear hysteretic loop emerges, with qualitatively similar features for high (upper panel) and low (lower panel) values of v_{ext}. Interestingly, and somewhat unexpectedly, the hysteretic regions are systematically broader for larger sliding velocities v_{ext}. We will return to this point later on.

The exact plateau state implies a kind of *dynamical incompressibility*, namely identically null response to perturbations or fluctuations trying to deflect the CM velocity away from its quantized value. Indeed, as long as F_{ext} remains below a critical threshold $F_c^{+\uparrow}$, it does perturb each individual single-particle motion, but has no effect whatsoever on v_{cm}, which remains exactly pinned to the quantized value, as is indeed expected of an incompressible state. This behavior contrasts with all observed non-plateau sliding states, where v_{cm} increases monotonically with F_{ext}. This plateau state is reminiscent of the pinned state of static friction, where a minimum force (the static friction force) is required to initiate the motion. Except that here in the starting "pinned" plateau state the lubricant chain particles are *moving* relative to both substrates. The sudden upward jump of v_{cm} taking place at $F_{ext} = F_c^{+\uparrow}$ can thus be termed
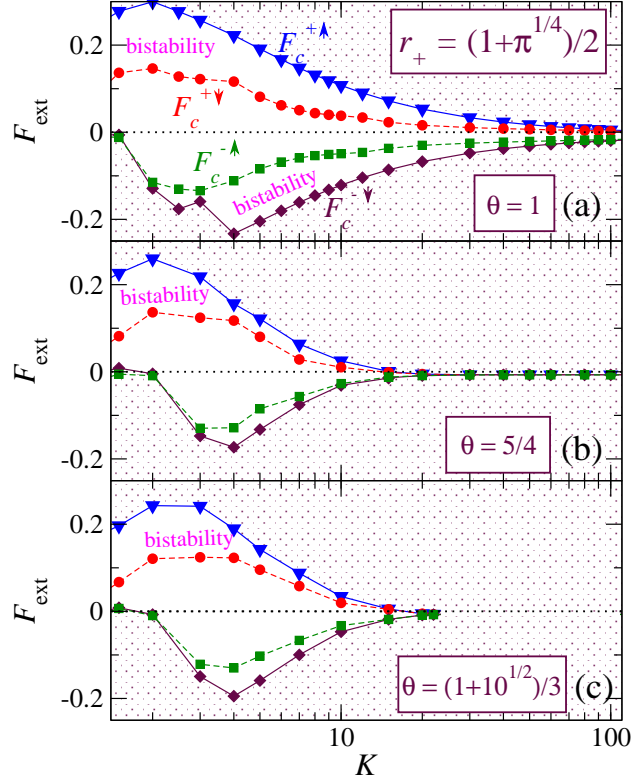
Figure 3. (Color online) The (K, F_{ext}) phase diagram illustrating the unpinning-repinning transitions for $r_+ = (1+\pi^{1/4})/2$, $\gamma = 0.1$, $v_{\text{ext}} = 0.1$, and for (**a**) one-to-one kink coverage $\theta = 1$; (**b**) commensurate kink coverage $\theta = 5/4$; (**c**) incommensurate kink coverage $\theta = (1 + 10^{1/2})/3$. The white areas have perfect plateau dynamics, the dotted region indicates quasi-free sliding. Simulations done with $N = 387$ particles for (**a**) and (**b**) and with $N = 781$ particles for (**c**).

a *dynamical depinning*. The depinning transition line $F_c^{+\uparrow}$, appears as a "first-order" line, with a finite jump Δv in the average v_{cm} and a clear hysteretic behavior: as F_{ext} is reduced back, the depinned state survives below $F_c^{+\uparrow}$ down to a significantly smaller $F_c^{+\downarrow}$, where perfectly quantized plateau sliding is retrieved, as illustrated in Fig. 2. Several hysteretic loops are in fact observed in Fig. 2: a qualitatively similar multi-step behavior appears also for $\theta = 1$ and $\theta = (1+10^{1/2})/3$. We shall return below to the nature of these steps. The large-F_{ext} quasi-free sliding regime is characterized by v_{cm} increasing continuously, roughly proportionally to F_{ext}/γ, and superposed to this general translational motion, by chaotic single-particle movements, contrasted to the periodic ($\theta = 1, 5/4$) or quasi-periodic ($\theta = (1 + 10^{1/2})/3$) individual-particle oscillations in the plateau state.

The values of $F_c^{+\uparrow}$, $F_c^{+\downarrow}$, and Δv are nontrivial functions of the parameters. Specifically, Fig. 3 reports the K dependency of these critical forces in the three considered cases. The values of the critical forces are remarkably similar for $K < 4$, while important differences are observed as the springs become stiffer. In particular, for unity coverage ($\theta = 1$) the plateau is very stable and extends to very large K, as expected in a fully commensurate case, see Fig. 3(a). In contrast, for noninteger θ the plateau becomes more fragile for large K. For commensurate $\theta = 5/4$ the plateau width decreases with some fast power law of K, and becomes numerically difficult to detect beyond $K \simeq 60$. For incommensurate $\theta = (1 + 10^{1/2})/3$ instead, the plateau shrinks and disappears at finite $K = K_{\text{Aubry}}^{\text{dyn}} \simeq 24$: no sign of a quantized plateau is detectable, e.g., for

$K = 25$. This unequal behavior for commensurate/incommensurate coverage θ is understood in terms of the mapping of the dynamical sliding model to the static FK model, which was established in Ref. [14]. The hysteretic depinning transition is observed through a significantly wide K-range in all three cases, but the depinning mechanism differs in some important detail.

3.1. Fully commensurate $\theta = 1$

As illustrated in Fig. 3, for $\theta = 1$ the plateau extends to very large K, in a range of F_{ext} of decreasing width $\propto K^{-1}$. K^{-1} describes precisely the asymptotic decrease of the sinusoidal interparticle distance modulation, residual after solitons overlap one another in the large K limit. For very large K, outside the right end of Fig. 3(a), the asymptotic values of this $F_c^{+\uparrow}$ curve lie entirely in the negative-F_{ext} domain. The explanation is that it takes a negative external force to compensate the positive average dissipative "wind" force $F_{\text{w}} = -2\gamma(v_{\text{cm}} - v_{\text{w}})$ acting on each lubricant particle. On the plateau state this wind force amounts to

$$F_{\text{w}} = -2\gamma\left(v_{\text{plateau}} - v_{\text{w}}\right) = \frac{2 - r_+}{r_+}\,\gamma\,v_{\text{ext}}\,. \tag{4}$$

In the absence of the external driving F_{ext}, the wind force alone is sufficient to disrupt the plateau at large K, where it is more fragile, as seen at the large-K side of Fig. 1. However, once F_{w} is compensated away, the $\theta = 1$ quantized plateau extends to indefinitely large K.

The next result concerns hysteresis, still at $\theta = 1$. Depinning is discontinuous and hysteretical as exemplified in Fig. 2, but only up to a large but finite critical stiffness $K = K_* \simeq 330$. Near K_* the bistability range $F_c^{+\uparrow} - F_c^{+\downarrow}$ closes up with a power law $F_c^{+\uparrow} - F_c^{+\downarrow} = B\,(K_* - K)^\alpha$, not unlike what was observed in previous work for the golden-mean ratio Ref. [14]. Above the critical stiffness, for $K \geq K_*$, $F_c^{+\uparrow} \equiv F_c^{+\downarrow}$, the depinning transition is continuous and characterized by what appears to be a mean-field power law $v_{\text{cm}} - v_{\text{plateau}} \propto (F_{\text{ext}} - F_c^{+\downarrow})^{1/2}$. For K approaching K_* from below, the plateau is abandoned through different mechanisms depending on the model parameters. In Ref. [16] it was found that re-pinning in the continuous sine-Gordon model proceeds first through a series of "cavity-mode" states, and then a series of kink-antikink wave train states, and a similar scenario is exhibited also by the discrete FK chain [15]. We find that analogous phenomena occur here for the repinning to the dynamical plateau, with defects in the kink lattice taking the place of the kink-antikink pairs of the single-chain FK model.

For soft enough chains, individual kinks are visible and well distinct. For example Fig. 4 (decreasing F_{ext}) illustrates the mechanism supporting deviations from the plateau for $K = 5$, the same value as Fig. 2. A kink vanishes at a $(-)$ lattice site and joins a second kink to form a mobile "bi-kink". This extra density accumulation "binds" substantially less than a kink to the minima of the $(-)$ potential. The external force F_{ext} acts on the bi-kink density lump and drags it along to the right. Contrary to the bi-kink, the site with a missing kink ("no-kink") remains pinned to the $(-)$ potential well, and is not dragged by the external force F_{ext}. The moving bi-kink breaks the "quantized" motion by one single particle, and is responsible for displacing the lubricant CM velocity a little bit away from the exact v_{plateau}.

The number of bi-kink – no-kink pairs tends to increase rapidly with increasing $F_{\text{ext}} - F_c^{+\downarrow}$. The force $F_c^{+\uparrow}$ necessary to nucleate the first bi-kink – no-kink pair is sufficiently large to sustain an avalanche of more bi-kink – no-kink pairs after the first defect is nucleated. Trains of bi-kinks cross the chain, producing essentially chaotic motions of the single lubricant particles, provided that $F_{\text{ext}} \gg F_c^{+\downarrow}$. When, starting from this dislodged, or depinned state, F_{ext} is gradually reduced, bi-kink – no-kink pairs annihilate, the number of these pairs reducing steadily with time. The discrete, integer nature of the defect-pair number originates the (gently sloping) discrete downward staircase steps in the hysteresis loop, generally similar to those shown in Fig. 2 (for a different θ). Since the discrete effect of the disappearance of a single defect-pair becomes negligible in the infinite-size limit, the observed multi-step structure appears to be
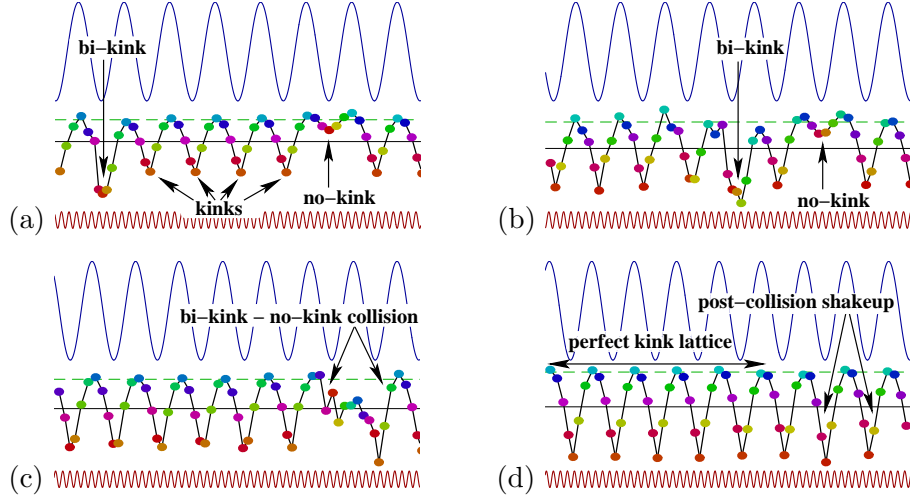
Figure 4. (Color online) Soft chain ($K = 5$). Four snapshots of a 60-particles section of the lubricant chain and $(+/-)$ substrates (lower/upper sinusoids), at successive times separated by 14 time units $(a_+ m/F_+)^{1/2}$. The horizontal direction represents distance, the dots the particle positions x_i. Vertical displacements of dots measure the distance $x_i - x_{i-1}$ of a given particle to its left neighbor: on this scale, the horizontal solid and dashed lines indicate the average interparticle distance a_0, and the $(+)$ lattice parameter a_+ respectively. The snapshots refer to $r_+ = (1 + \pi^{1/4})/2$, $\theta = 1$, $F_{\text{ext}} = 0.08136$ (decreasing), and illustrate the crossing of the critical line $F_c^{+\downarrow}$, with the recovery of the plateau state (see Fig. 2) occurring through the disappearance of the last bi-kink – no-kink defect. The other parameters are $\gamma = 0.1$, and $v_{\text{ext}} = 0.1$. This annihilation of a bi-kink against a stationary no-kink is best illustrated by the online animation repinning_theta1_K5.gif, which spans 70 time units, starting 11 time units before frame (a) and ending 17 time units after frame (d) of the present figure. For this and all animations we select the reference frame where the $(-)$ substrate, and thus all pinned kinks, are stationary.

merely a finite size artifact, and for all that we can tell at present the infinite system should exhibit no staircase steps. In the depinned state, so long as F_{ext} is strong enough, a bi-kink encounters a no-kink, interacts briefly, and then continues to travel. When instead F_{ext} is reduced below $F_c^{+\downarrow}$, as in Fig. 4, the encounter of a bi-kink and a no-kink leads to reciprocal annihilation. The amplitude oscillation still visible (but quickly damped) at the right end side of the last frame of Fig. 4 reflects the waves dissipating the excess ("binding") energy of the bi-kink – no-kink pair, in the process of recovering the perfect kink lattice. When finally the kink lattice gets rid of the last defect pair, the perfect plateau state is re-gained.

For a stiff enough chain, individual kinks become spatially broad, and will for a fixed density extend over a size larger than the average inter-kink distance $a_+/(r_+ - 1)$. In this limit the kink lattice reduces to a weak sinusoidal deformation, of amplitude $\propto K^{-1}$ superposed to the average interparticle density. Despite this difference with the strong kink lattice of the soft-chain case, the external-force–induced departure from the quantized velocity plateau occurs here through a mechanism similar to that illustrated above for the soft-spring case. A chain slippage by one particle (i.e. a distance a_0) is promoted by a bi-kink and a no-kink moving in opposite directions: when they collide, the bi-kink – no-kink pair takes the aspect of a broad locally flat region of denser-than-average and less-dense-than-average lubricant in the otherwise perfect pinned kink lattice. As illustrated in Fig. 5(a), a local flattening defect forms in the soliton lattice, similar to the local amplitude suppression of a dragged charge density wave (CDW) [18, 19]. This defect is characterized by a smooth "charge" separation, with the denser region being driven to the
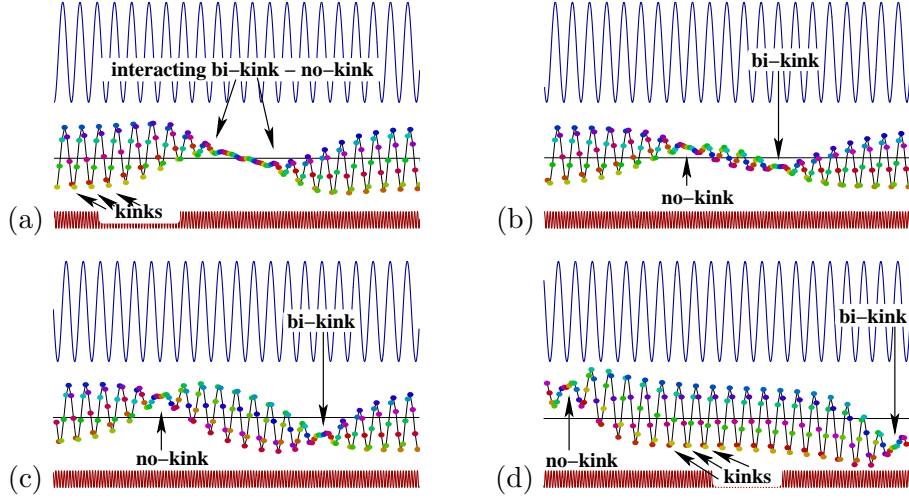
Figure 5. (Color online) Stiff chain ($K = 50$). Four successive snapshots of the substrates and lubricant chain, separated by time intervals of 9 model units. All notations and parameters are the same as in Fig. 4, except for $K = 50$, $F_{ext} = 0.00685$ (decreasing), which falls in the region immediately above the critical line $F_c^{+\downarrow}$, before the recovery of the plateau state. The complete collision of the right-traveling bi-kink and left-traveling no-kink is best illustrated by the online animation unpinned_theta1_K50.gif, which spans 50 time units, starting 16 time units before frame (a) and ending 7 time units after frame (d).

right and the more rarefied region to the left by the driving force, the external force acting like an electric field on a CDW insulator. These defects travel in opposite directions, as expected of a opposite charges driven by an electric field. The crucial difference with the soft-spring case (where as shown by Fig. 4, the no-kink defect remains pinned to the ($-$) lattice) is that here both defects, the by-kink and the no-kink, are mobile and dragged by the external force. As the two defects move apart, a perfect soliton lattice re-forms in between, Fig. 5(d). In time, a right-moving bi-kink encounters a left-moving no-kink: these defects may again cross, or else they may bind and annihilate in pairs. Annihilation occurs when F_{ext} is reduced below $F_c^{+\downarrow}$, as in the soft-chain case of Fig. 4. When instead, $F_{ext} > F_c^{+\downarrow}$ the pair separates again, with the rightward "positive" and leftward "negative" flattenings suffering some phase shift, but traveling on, as in Fig. 5. As soon as all defects annihilate, the kink lattice is perfect, and the CM velocity recovers $v_{plateau}$ exactly. If the defect pairs form at regular spatial separation within the chain (with periodic boundary conditions) the corresponding moving pattern leads to time-periodic fluctuations of the CM velocity; that can also be seen as type-I intermittencies [20]. Otherwise, when defect motion is chaotic, an irregular CM dynamics is observed. For indefinitely growing chain stiffness K, each defect pair flattening region grows in size, eventually covering the entire finite-size simulation, which becomes at that point a poor representation of the infinite-size thermodynamical limit.

Figure 6 draws the plateau boundaries relative to F_{ext}, for varied external driving v_{ext}, for a rather stiff chain ($K = 50$). As the friction-drag reference force F_w grows linearly with v_{ext}, and this introduces a trivial compensating trend $F_c^{\pm\uparrow/\downarrow} \propto -F_w$, it is convenient to remove the appropriate linear drift by adding F_w, Eq. (4), to the critical forces. The static limit $v_{ext} = 0$ is smooth, and this indicates a regime of continuity from the static quasiperiodic 3-lengthscale model of Ref. [21] to the dynamical sliding. Strikingly, the plateau robustness against the external perturbing force F_{ext} and the widths of the hysteretical regions *benefit* of increased driving speed. For large $v_{ext} \simeq 7$ the plateau destabilizes suddenly and eventually disappears.
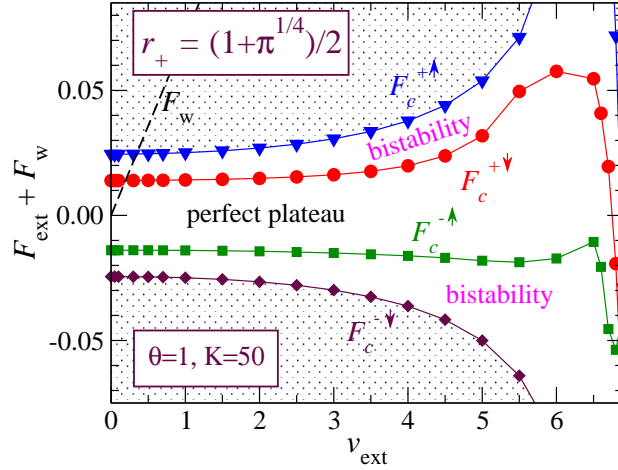
Figure 6. (Color online) Driving-velocity dependency of the dynamical depinning and repinning forces $F_c^{+\uparrow}$ $F_c^{+\downarrow}$, $F_c^{-\downarrow}$ $F_c^{-\uparrow}$ (shifted upward by the trivial $F_{\rm w} \propto v_{\rm ext}$ contribution, Eq. (4)). $v_{\rm ext}$ is measured in model units of $(F_+ a_+/m)^{1/2}$; the chain is rather hard ($K = 50$); $r_+ = (1 + \pi^{1/4})/2$, $\theta = 1$ ($r_- \simeq 7.036$), and $\gamma = 0.1$.
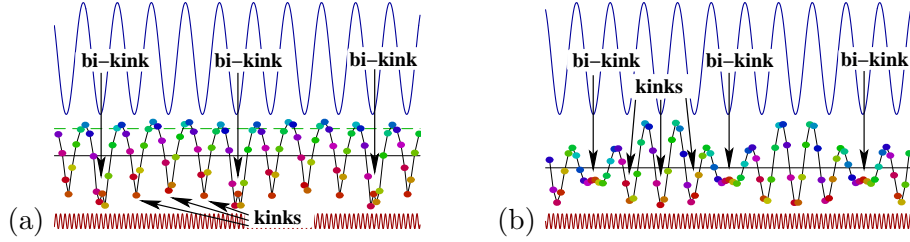

Figure 7. (Color online) Typical plateau arrangements of the $\theta = 5/4$ commensurate soft $K = 5$ (a) and hard $K = 50$ (b) chain: a regular arrangement of bi-kinks (one every four kinks). The conventions and all other parameters are the same as in Fig. 4, but for $F_{\rm ext} = -F_{\rm w}$.

3.2. Commensurate $\theta = 5/4$

Having explored at length the $\theta = 1$ commensurability, we now turn to another kink lattice/slider system, still commensurate but with $\theta = 5/4$, a weaker commensurability than $\theta = 1$. At $\theta = 5/4$, in the perfect-plateau state one kink out of four turns into a bi-kink, as illustrated in Fig. 7. (The bi-kinks of the present $\theta > 1$ case would be replaced by no-kinks for $\theta < 1$). The pre-existence of a regular array of such defects of the kink lattice allows for a significantly different depinning mechanism, compared to the totally commensurate $\theta = 1$ case. Defects of the kink lattice are already present prior to turning on the external force $F_{\rm ext}$, which only sets them into motion, without a need to create them. For soft springs, Fig. 7(a), where the pinning energy barrier of these defects is large, Fig. 3 shows that the critical forces needed to set the defects into motion in this $\theta = 5/4$ case are very similar to those for $\theta = 1$. For harder springs, defects increase in size and affect several neighboring kinks now, as illustrated in Fig. 7(b). These extended disturbances possess a much smaller pinning energy to the $(-)$ potential. As a consequence, the plateau state is now exceedingly weak, confined to an extremely narrow force range around $-F_{\rm w}$, see Fig. 3. The ordered arrangement of defects still warrants some amount of pinning, but the width $F_c^{+\uparrow} - F_c^{-\downarrow}$ of the pinned region decreases much faster than in the $\theta = 1$ case as soon as the defect size exceeds the typical inter-defect distance $a_+/(r_+ - 1)/\theta$, here occurring for $K \simeq 10$.
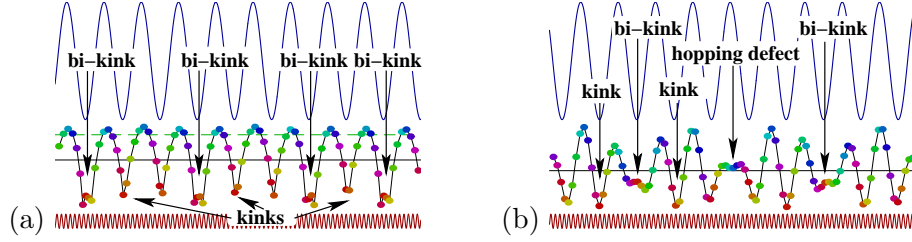
Figure 8. (Color online) $\theta = (1 + 10^{1/2})/3$ incommensurate soft chain $K = 5$ (a) and hard chain $K = 50$ (b): irregular alternation of kinks and bi-kinks. Pinning is realized for the soft chain, while even with $F_{ext} = -F_w$, so that $v_{cm} \simeq v_{plateau}$, the $K = 50$ hard chain is unpinned, with the defects slowly drifting along. The conventions and all other parameters are the same as in Fig. 4. The online file unpinned_incommensurate.gif provides an animation of the situation of snapshot (b). A second multimedia file, unpinned_incommensurate_drifting.gif, shows the defects drifting under the effect of a deviation of F_{ext} by 10^{-3} force units in excess of $-F_w$.

3.3. Incommensurate $\theta = (1 + 10^{1/2})/3$

Finally, at irrational $\theta = (1 + 10^{1/2})/3$, some kinks are replaced by bi-kinks, but the incommensuracy of the coverage leads to their irregular arrangement, as illustrated in Fig. 8. For a sufficiently soft chain, (represented by $K = 5$ in Fig. 8(a)), the irregular distribution of single kinks and bi-kinks remains statically pinned to the minima of the $(-)$ substrate, with a finite barrier to overcome for a bi-kink to migrate to the next minimum. This barrier guarantees the existence and robustness of the CM quantized velocity plateau (with a first-order hysteretical boundary) in the present incommensurate case, pretty much like for the commensurate cases. This energy barrier protects the plateau against the movement of bi-kinks until $K < K_{Aubry}^{dyn} \simeq 24$. In contrast, for a harder chain ($K > K_{Aubry}^{dyn}$), illustrated by $K = 50$ in Fig. 8(b), the irregular distribution of single kinks and bi-kinks drifts through the chain at a speed approximately proportional to $F_{ext} + F_w$, with no sign of any pinned plateau: this indicates that the energy barrier is here entirely removed by the irregular bi-kink configuration produced by incommensuracy. The kink-kink repulsion makes the bi-kinks increasingly extended objects as K increases, until they become so broad that crossing the maxima of the $(-)$ potential costs negligible energy: the bi-kink in the central region of Fig. 8(b) exemplifies precisely one such slow hopping process. The transition between the soft-chain dynamically pinned regime and the stiff-chain fully unpinned state is analogous to the Aubry transition observed in the static situation described by the FK model. The kinks of the dynamical model play the role of the particles of the static model.

3.4. Hysteresis when cycling other parameters

By analogy to the single-chain FK model, cycling the external force F_{ext} is conceptually the most natural way to abandon and recover, often hysteretically, the dynamical plateau. However, in practice, the experimental realization of a uniform force acting equally on each lubricant particle in flight is not trivial. On the other hand, the plateau can be abandoned and recovered, even when different parameters are cycled. Within the present model, the reason is that the dissipation γ-term has itself the effect of diverting the CM velocity away from $v_{plateau}$. In a concrete laboratory configuration moreover, beside dissipative effects, other interactions too will tend to push the lubricant slide at speeds other than $v_{plateau}$. As an example, defects and grain boundaries will tend to pin statically the lubricant to either substrate [22]. These other "external" forces compete with the tendency to dynamical pinning: the latter tuned by other parameters, namely, in the language of our model, K F_+ F_- and v_{ext}. Thus in a practical
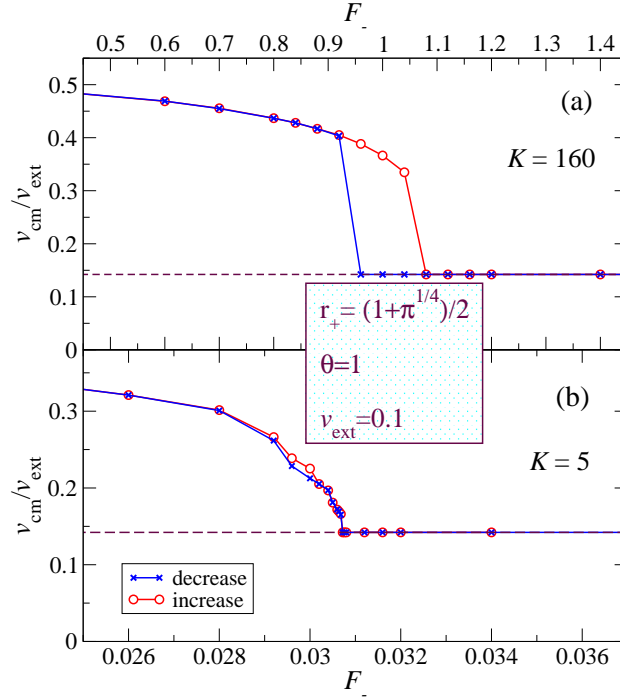
Figure 9. (Color online) Hysteresis loops found as the corrugation of the $(-)$ substrate F_- is cycled down from (crosses) and back up to (circles) its value F_+ used in all other calculations. (a) At $K = 160$, near the plateau edge of Fig. 1, it takes a small decrease in F_- to leave the plateau, while (b) when the plateau is very robust $(K = 5)$, nonhysteretic depinning is observed for a corrugation amplitude F_- far below unity. Simulations for $r_+ = (1 + \pi^{1/4})/2$, $\theta = 1$ $(r_- \simeq 7.036)$, $\gamma = 0.1$, $v_{\text{ext}} = 0.1$.

straightforward experiment, cycling quantities such as the the sliding speed, or the load applied to the sliders should lead to leaving/recovering the plateau dynamics, with hysteretic cycles similar to those exemplified by Fig. 2.

To illustrate this point within our model, Fig. 9 depicts a first example of such a hysteretic cycle, where the load applied to the sliders, proportional to the upper slider corrugation F_-, is cycled. The plateau is abandoned hysteretically when F_- is decreased below critical values which depend strongly on the robustness of the pinned state, which is, in turn, a function of K and other model parameters.

Along a similar scheme, the perfectly legitimate interpretation of Fig. 6 as a phase diagram suggests that the first-order line separating the free-sliding regime from the perfect plateau could be crossed by cycling v_{ext} rather than F_{ext}. This cycle corresponds to tracking up and down the $F_{\text{ext}} = 0$ dashed path drawn in Fig. 6. The resulting loop, shown in Fig. 10(a), depicts the expected bistability: v_{ext} is cycled up and down, and the perfect plateau is abandoned at much larger speed than where it is recovered. At large speed F_{w} increases, the dissipative term dominates and makes the lubricant speed approach v_{w}.

The depinning transition may also occur continuously, when the transition line is crossed beyond the tricritical point, i.e. for $K > K_*$, in the strongly dissipative region, where the the viscous damping rate γ/m is much larger than the vibrational frequencies, decreasing proportionally to K^{-1}, of the soft kink lattice around the minima of the $(-)$ potential. In this regime the dynamical depinning is apparently second order. In this overdamped regime, shown for example in Fig. 10(b), the forward and backward trajectories become indistinguishable, and
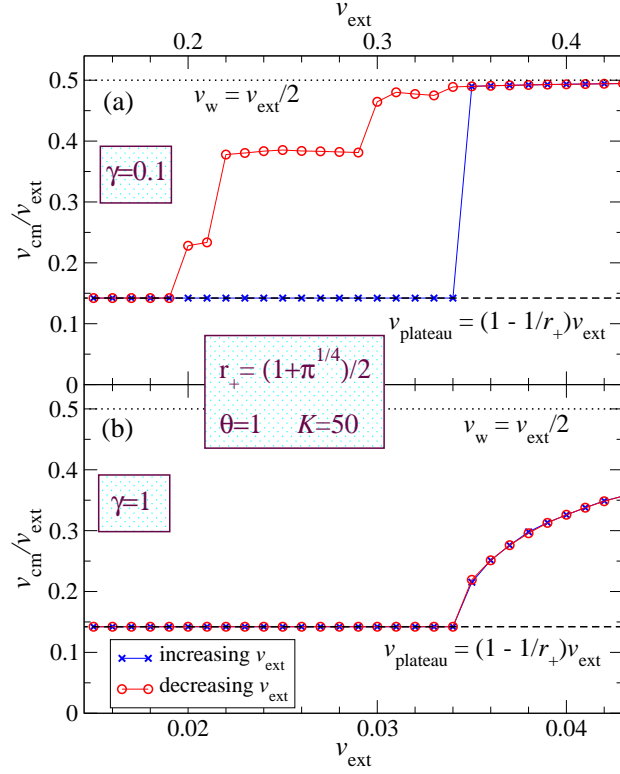
Figure 10. (Color online) (a) Hysteresis loop at the plateau edge in the $v_{\text{cm}} - v_{\text{ext}}$ characteristics for a confined chain of length ratios $r_+ = (1 + \pi^{1/4})/2$, $\theta = 1$ ($r_- = 7.036$). Adiabatic increase and decrease of v_{ext} are denoted by crosses and circles, respectively. Here $\gamma = 0.1 \, (F_+ m/a_+)^{1/2}$ and $F_{\text{ext}} = 0$, which corresponds to the dashed path of Fig. 6. (b) No hysteresis is observed in the overdamped regime ($\gamma = 1.0 \, (F_+ m/a_+)^{1/2}$) along the same path.

hysteresis disappears. In this strongly dissipative regime, we find, instead of the hysteretic jumps, a nonlinear dependency of v_{cm} versus the model parameters (here v_{ext}, but cycling F_{ext}, F_-, or K would lead to perfectly analogous results), without any bistability phenomena.

4. Discussion and conclusions

We have shown that starting from the quantized sliding plateau state, previously found for a simple tribological model of a confined layer, the sliding dynamics of the lubricant layer exhibits a large hysteresis when an additional external driving force F_{ext} trying to push v_{cm} away from its quantized value is cycled. In analogy to depinning in ordinary static friction [15], the hysteretic dynamical behavior depends strongly on whether the system degrees of freedom have sufficient inertia (underdamped regime) or if, on the contrary, inertia is negligible (overdamped regime). Hysteretic versus continuous depinning occurs depending on whether the unpinning transition is crossed below or above a tricritical point where hysteresis close, and which marks the separation between the underdamped and the overdamped dynamics.

Hysteresis arises due to the great robustness of the quantized dynamics, setting a large critical threshold $F_c^{+\uparrow}$ to the formation of mobile defects (initially depinned bi-kinks or no-kinks). Once at least one of these defects forms, an avalanche process leads to a discontinuous jump to a free or quasi-free sliding regime. Starting from the unpinned states, the plateau recovers only at a much smaller threshold $F_c^{+\downarrow}$, representing the minimum driving force needed to sustain the motion of pre-existing mobile defects.

Nontrivial differences with static friction occur. The first is that the dynamical pinning hysteresis cycle may be larger in situations where pinning itself could be intuitively considered more fragile, e.g., for larger external velocity. Another feature (presently under investigation, not discussed above) is that the *sudden* application of an external force can sometimes leave v_{cm} locked to the quantized value, even if the applied force is larger than the dynamic depinning threshold $F_c^{+\uparrow}$ obtained instead through the adiabatic procedure sketched above. Once again, this is different from static depinning, usually requiring smaller force (than the static friction F_s) if applied suddenly [5].

The present study concentrates on zero temperature. At finite temperature, the energy barrier to the formation of defects such as bi-kinks and for defects "hopping" to neighboring pinning sites can be traversed by means of random thermal excitations. This means that at sufficiently low temperature the dynamical pinning should not change much. Even the hysteresis should remain, provided that parameters such as F_{ext} are cycled much faster than the characteristic thermal relaxation times. Thermal effects are currently under closer investigation.

Acknowledgments

References

[1] T. Kapitaniak and J. Wojewoda, *Attractors of quasiperiodically forced systems* (World Scientific, Singapore, 1993).

[2] B. N. J. Persson, *Sliding Friction: Physical Principles and Applications (NanoScience and Technology)* (Springer-Verlag, Berlin 1998).

[3] S. M. Rubinstein, G Cohen, and J. Fineberg, Nature **430**, 1005 (2004).

[4] See, e.g., A. Vanossi and O. M. Braun, "Simulation of nanofriction through driven simplified models", to appear in *Advances in contact mechanics*, edited by R. Buzio and U. Valbusa (Research Signpost, Kerala, India), and references therein.

[5] O. M. Braun and Yu. S. Kivshar, *The Frenkel-Kontorova Model: Concepts, Methods, and Applications* (Springer-Verlag, Berlin, 2004).

[6] M. G. Rozman, M. Urbakh, and J. Klafter, Phys. Rev. Lett. **77**, 683 (1996); Europhys. Lett. **39**, 183 (1997).

[7] V. Zaloj, M. Urbakh, and J. Klafter, Phys. Rev. Lett. **81**, 1227 (1998).

[8] M. Dienwiebel, G. S. Verhoeven, N. Pradeep, J. W. M. Frenken, J. A. Heimberg, and H. W. Zandbergen, Phys. Rev. Lett. **92**, 126101 (2004).

[9] J. Y. Park, D. F. Ogletree, M. Salmeron, R. A. Ribeiro, P. C. Canfield, C. J. Jenks, and P. A. Thiel, Science **309**, 1354 (2005).

[10] O. M. Braun, A. Vanossi, and E. Tosatti, Phys. Rev. Lett. **95**, 026102 (2005).

[11] A. Vanossi, N. Manini, G. Divitini, G. E. Santoro, and E. Tosatti, Phys. Rev. Lett. **97**, 056101 (2006).

[12] G. E. Santoro, A. Vanossi, N. Manini, G. Divitini, and E. Tosatti, Surf. Sci. **600**, 2726 (2006).

[13] N. Manini, M. Cesaratto, G. E. Santoro, E. Tosatti, and A. Vanossi, J. Phys.: Condens. Matter **19**, 305016 (2007).

[14] A. Vanossi, N. Manini, F. Caruso, G. E. Santoro, and E. Tosatti, submitted to Phys. Rev. Lett. (2007).

[15] O. M. Braun, A. R. Bishop, and J. Röder, Phys. Rev. Lett. **79**, 3692 (1997).

[16] J. C. Ariyasu and A. R. Bishop, Phys. Rev. B **35**, 3207 (1987).

[17] A. Vanossi, G. E. Santoro, N. Manini, M. Cesaratto, and E. Tosatti, in press Surf. Sci. (2007); cond-mat/0609117.

[18] G. Grüner, Rev. Mod. Phys. **60**, 1129 (1988).

[19] M. Inui, R. P. Hall, S. Doniach, and A. Zettl, Phys. Rev. B **38**, 13047 (1988).

[20] P. Bergé, Y. Pomeau, and C. Vidal, *Order within Chaos* (Hermann and Wiley, Paris, 1984).

[21] A. Vanossi, J. Röder, A. R. Bishop, and V. Bortolani, Phys. Rev. E **63**, 017203 (2000).

[22] M. Cesaratto, N. Manini, A. Vanossi, E. Tosatti, and G. E. Santoro, in press Surf. Sci. (2007); cond-mat/0609116.